Corrosion Science 180 (2021) 109189

Contents lists available at ScienceDirect

Corrosion Science

journal homepage: www.elsevier.com/locate/corsci

Flash-PEO as an alternative to chromate conversion coatings for corrosion protection of Mg alloy

E. Wierzbicka [a,*], B. Vaghefinazari [b], S.V. Lamaka [b], M.L. Zheludkevich [b], M. Mohedano [a], L. Moreno [a], P. Visser [c], A. Rodriguez [d], J. Velasco [d], R. Arrabal [a], E. Matykina [a]

[a] Departamento de Ingeniería Química y de Materiales, Facultad de Ciencias Químicas, Universidad Complutense, 28040, Madrid, Spain
[b] MagIC—Magnesium Innovation Center, Helmholtz-Zentrum Geesthacht (HZG), 21502 Geesthacht, Germany
[c] AkzoNobel, Expertise Center Corrosion, Rijksstraatweg 31, 2171 AJ, Sassenheim, the Netherlands
[d] Fundación CIDAUT, Parque Tecnológico de Boecillo, 47151, Boecillo, Valladolid, Spain

ARTICLE INFO

Keywords:
Magnesium
Coating
Plasma electrolytic oxidation
Flash-PEO
Filiform corrosion
Pitting corrosion
Inhibitor

ABSTRACT

In the present work, a flash-PEO coating is developed on AZ31B alloy in a combination of silicate, phosphate, and fluoride based electrolyte in order to offer a green alternative to chromate conversion coatings. Multilevel active protection is achieved through synergetic combination of self-sealing effect of PEO coating itself and active inhibition provided by an organic inhibitor impregnated in PEO pores in a post-treatment step. The results indicate that flash-PEO coatings, loaded with organic corrosion inhibitors, can be recommended for exploitation on industrial level as an equally effective corrosion protection system alternative to CCC for paint-bearing and paint-free applications.

1. Introduction

Mg alloys are of big interest for automobile and aircraft industries. Light metals application is a common approach to reduction of operating costs, increase of vehicle payload and reduction of environmental impact in order to meet stringent emission regulations.

The biggest challenge for Mg alloys application is adequate corrosion protection. Mg is a very active metal whose low corrosion resistance is predetermined by its standard electrode potential of E=-2.37 V_{SHE} that makes it highly susceptible to galvanic corrosion in a presence of second phases in the alloys. Additionally, the magnesium oxide/hydroxide film that forms on the surface is only partially protective when exposed to neutral saline environments.

Since early 1920s, chromate-based coatings have efficiently been used for corrosion protection of various types of alloys, including steel, galvanized steel, Mg and Al. For a long time, there was no other equally efficient alternative coating nor dedicated technology for light metals. However, according to recent REACH regulation Cr(VI) which is highly toxic and carcinogenic must be withdrawn from use and replaced by new environmental-friendly substitutes equally effective in terms of corrosion and paintability performance.

An alternative Cr-free anticorrosive coating technology that deserves particular attention is plasma electrolytic oxidation (PEO) or micro-arc oxidation (MAO). This is an electrochemical surface treatment that operates above the so-called dielectric breakdown voltage, resulting in numerous short-lived plasma microdischarges at the metal surface [1,2]. As a result of a complex combination of electrochemical, plasma-chemical and oxidation reactions, a well-adhered and thick oxide coating is formed. This typically exhibits a three-layer structure comprising a top porous region, an intermediate compact layer and a thin barrier layer [3–6]. Advantages of PEO technology include fast coating growth rate and very good paintability owed to the top porous layer [7].

High voltages (~300−400 V) are a prerequisite of the PEO treatments which typically last between 15 and 30 min. These factors elevate the cost of the treatment, thereby greatly limiting implementation of PEO technology to industrial mass-scale production [8,9]. An alternative explored in this work is to employ short treatment times in order to produce "flash"-PEO coatings. The term "flash" refers not as much to the thickness of the coating as to the very short duration of the process [10–12]. Limiting the PEO treatment time to 1 min only should produce cost-effective coatings with thicknesses and corrosion protection comparable to chromate conversion coatings (CCCs).

The composition and concentration of the electrolyte play a crucial

* Corresponding author.
E-mail address: ewierzbi@ucm.es (E. Wierzbicka).

https://doi.org/10.1016/j.corsci.2020.109189
Received 21 September 2020; Received in revised form 23 November 2020; Accepted 10 December 2020
Available online 14 December 2020

role in the composition and corrosion resistance of PEO coatings, since electrolyte species readily incorporate into the coatings during plasma micro-discharges [13,14]. Most typically, KOH or NaOH are used to ensure an alkaline environment (necessary to carry out PEO). Phosphates, silicates, fluorides or aluminates are added, often in combined formulations, to passivate the substrate and improve the coating corrosion resistance. In particular, fluorides are known to have a beneficial impact on corrosion resistance due to formation of sparingly soluble MgF_2 which ennobles the corrosion potential [15–18]. Also, relevant is the incorporation of phosphorus species in the coatings [19–22] since they have been reported to provide a self-repairing mechanism at coating damaged sites [23]. The porous structure of PEO coatings can be exploited as a reservoir for corrosion inhibitors in order to further improve the corrosion protection properties of PEO coatings. The active protection efficacy of organic and inorganic inhibitors loaded into the pores of thin PEO coatings and sealed with a top sol-gel layer was demonstrated [24–29].

In the present work, a combination of silicate, phosphate and fluoride based electrolyte is used to achieve a synergetic inhibitive effect of a thin PEO coating on corrosion of Mg AZ31B alloy. Multilevel active protection was further ensured through impregnation of the flash-PEO coating with an organic corrosion inhibitor following a screening procedure of several candidates and painting with an inhibitor-loaded epoxy primer. Full system protection was verified in a standardized paint adhesion and neutral salt spray tests (NSST) in comparison with CCC with a chromate-loaded primer. The results indicate that flash-PEO coatings in combination with active corrosion inhibitors have a solid chance to rank in the leading position of green Mg corrosion protection technologies.

2. Materials and methods

2.1. PEO and CC coatings fabrication

Magnesium alloy AZ31B 1.5 mm-thick sheet (SMW Engineering, wt. %: 0.0028Fe, 0.0103Si, 0.24Ce, 0.76Zn, 0.0008Ca, 0.19 Mn, 2.72Al, Mg bal.) cut into 40 × 40 mm specimens and 75 × 250 mm coupons was used as a substrate for PEO treatment. To clean and pre-treat the sample surface a two-step commercial procedure was used. This consisted of 15 min treatment at 80−90 °C in alkaline surfactant solution (Bonderite C—AK 4181 L, 90 g/L), followed by 4 min of acidic etching in H_2SO_4-based solution at room temperature (Bonderite C—IC 3610, 10 g/L) which maintained the supplier-recommended etching rate of Mg substrate above 10 g/m^2. A DC power supply (Delta Elektronika SM 400-AR-8) with computer-controlled regulation of the process conditions and current and voltage signal acquisition was used for PEO treatment. The electrolyte, further referred to as SiPF, contained 2.8 g/L KOH, 5 g/L Na_2SiO_3, 5 g/L Na_3PO_4 and 3 g/L KF (pH 12.5, conductivity 23.9 mS/cm). Anodizing was carried out under continuous stirring in a 2 L thermostated (20 ± 1) ºC double-walled glass cell using a 316 L stainless steel mesh cylinder as a counter electrode and an insulated copper wire for electrical contact. A constant current density of 100 mA/cm^2 was applied, a voltage limit V_{fin} was set at 350 V and treatment time was limited to 60 s. After the treatment, the specimens were rinsed sequentially with deionized water and isopropanol followed by drying in warm air.

Up-scaling of flash-PEO treatment to 75 × 250 mm coupons (**Supplementary** Fig. 1) was performed in a 50 L tank with two 250 × 400 mm 316 L stainless steel cathodes using a MAGPLUS QP-800/60/1000 bipolar power supply (MAGPLUS Stromversorgungs Systeme GmbH, Germany) operated in a DC mode. The electrical connection was made at two points using commercially pure (c.p) Ti screws (4 mm ∅ thread size). The following adjustments of electrical parameters were required in order to compensate for the larger inter-electrode distance and ohmic drop that occurs in a 50 L tank and achieve the same coating thickness as in lab-scale specimens: (i) a current density increased to 110 mA/cm^2 ; (ii) the treatment time limited to 75 s; (iii) the maximum voltage limited to 315 V.

2.2. Inhibitors screening, incorporation into the PEO coating and sealing

Ten different inhibitors were evaluated through H_2 evolution test on the pre-treated bare AZ31 to find 4 best-performing inhibitors to be incorporated into the PEO coating. The inhibitors were chosen from a comprehensive database of the inhibitors published in [30]. The details of the screening step and its results are provided in supplementary materials of this work. Four inhibitors, screened to be incorporated into the PEO coatings, are: 4Methylsalicylate-Na, 3Methyl2Nitrobenzoate-Na, 2,5PDC-Na, Quinaldate-Na.

Incorporation of the inhibitors into the PEO pores was carried out by immersion of the samples in the inhibitor solution at low-pressure condition. Inhibitor solutions were prepared by dissolution of 0.05 M inhibitor in deionized water followed by pH adjustment to the value of 7.0 ± 0.2 by NaOH, except for 3-Methyl-2nitrobenzoate-Na solution which was adjusted to pH of 9.0 ± 0.2. The solution, along with the immersed sample, was placed in a well-sealed chamber. A water-jet vacuum pump was employed to reduce the pressure inside the chamber to approximately 0.9 bar in order to release the air entrapped inside the PEO pores into the solution. The low-pressure conditions were maintained for 20 min until no visible bubbles could be observed on the sample surface. The inhibitor-loaded samples were flushed fast with deionized water and dried using a warm flow of air.

A ~25 μm-thick layer of 3-component epoxy inhibitor-free primer (276:87:85 g of Epoxy Primer 37076 : Hardener 92133 : Thinner C25/90S, supplied by AkzoNobel) was applied on one side of 40 × 40 mm specimens with a drawbar. Paint was cured at 80 °C for 1 h. The 75 × 250 mm coupons with inhibitor loaded flash-PEO coating and a reference CCC coating (MTU Aero Engines, Germany) were both sides coated by AkzoNobel using following industrial epoxy primers: non-inhibiting epoxy chromate free primer, a chromated reference primer and a state-of-the-art chromate-free primer with active inhibition based on lithium leaching technology [31]. The latter primer was included into the scaled-up testing batch as a current green commercial alternative to chromate-based primers. Likewise, a reference CCC-coated coupons (MTU Aero Engines, Germany) were painted with industrial qualified chromate-containing epoxy primer.

2.3. Coating characterization and corrosion testing

Coating thickness was measured using an eddy-current meter (ISOSCOPE FMP10, Fischer), equipped with an FTA3.3H probe, taking an average of 10 measurements. The electrochemical impedance spectroscopy (EIS) measurements were performed using a computer controlled GillAC (ACM Instruments) potentiostat and a three-electrode cell in 0.5 wt% NaCl solution. The defined working area of the tested electrode was 1 cm^2; the counter and reference electrodes were respectively graphite and silver/silver chloride (Ag/AgCl in 3 M KCl). The open circuit potential (OCP) was allowed to stabilize before the measurements for 15 min. Summary of OCPs registered directly before the EIS in presented in **Supplementary** Table 1. In order to evaluate the effect of longer exposure time of the coatings, the samples were immersed during 24 h, 48 h, 72 h and 1 week before EIS measurements. The measurements were carried out over a frequency range from 30 kHz to 10 mHz (50 points in total), using a 10 mV amplitude sinusoidal

Table 1
Samples types and conditions of conducted NSST according to ASTM B117 standard in a 5% NaCl fog.

	Coating	Inhibitor	primer	Scratch size [mm]	NSST duration	Figure
Lab scale samples 40 × 40 mm	CCC	–	non-inhibiting epoxy chromate-free	15	168 h	9
	SiPF	–				
		4Methylsalicylate-Na				
		3Methyl2Nitrobenzoate-Na				
		Quinaldate-Na				
		2,5PDC-Na				
	CCC	–				13
	SiPF	–				
	SiPF	4Methylsalicylate-Na				
	SiPF	–		–	2000 h	14
	SiPF	4Methylsalicylate-Na				
Large size coupons 75 × 250 mm	CCC	–	–	–	168 h	15
	SiPF	4Methylsalicylate-Na				
	CCC	–	non-inhibiting epoxy chromate-free	–	1000 h	
	SiPF	4Methylsalicylate-Na				
	CCC	–	chromated			
	SiPF	4Methylsalicylate-Na	chromate-free with active inhibition			
	CCC	–	non-inhibiting epoxy chromate-free	50 × 50		
	SiPF	4Methylsalicylate-Na				
	CCC	–	chromated			
	SiPF	4Methylsalicylate-Na	chromate-free with active inhibition			

signal. Each measurement was repeated at least twice each time using a new specimen. The spectra fitting was performed using a ZView software, ensuring the goodness of fit by chi-squared values in the range of 0.001–0.0001. The errors for the individual parameters of the equivalent electrical circuits (such as CPE and R) were <5%.

The plan view and cross-sectional coatings morphologies were examined using scanning electron microscopy (SEM, JEOL JSM-6400) equipped with energy dispersive X-ray (EDS) microanalysis facility. Elemental composition was determined as an average of the analyses of three different areas. The cross-sections of the specimens embedded in epoxy resin were prepared by grinding gradually with SiC abrasive paper from P120 to P1200 grade and followed by diamond paste finish to 0.1 μm. Crystalline phases in the coating were determined using Philips X'Pert MRD X-ray diffractometer (Cu Kα =1.54056 Å) operated in a grazing angle mode from 10° to 90° 2θ with an incidence angle of 1°, step size 0.04° 2θ and counting time 15 s/step.

Surface texture was studied with a focus variation optical profilometer with a ×50 lense (Alicona InfiniteFocusSL).

Fourier transform infrared spectroscopy (FTIR) analysis was performed using a Nicolet iS50 instrument equipped with a KBr beamsplitter and a DTSG-KBr detector. ATR SpectraTech Performer with a diamond crystal was utilized. The measurements were performed using 128 scans at 4 cm^{-1} resolution. Additionally, MicroFTIR analysis was carried out using a Nicolet iMX10 spectrophotometer with KBr beamsplitter KBr and MCT/A detector refrigerated with liquid air. Measurement were performed with germanium crystal MicroATR accessory, 256 scans and 8 cm^{-1} resolution.

Active protection effect of prepared coatings was studied by monitoring local current densities by Scanning Vibrating Electrode Technique (SVET). Three samples were prepared including CCC treated, flash-PEO treated SiPF and that with incorporated corrosion inhibitor (SiPF-4MSA). None of the three samples for SVET measurements was coated with a primer. The area monitored by SVET was ca. 4.0 × 4.0 mm for each sample. The remaining surface of the samples including the edges was insulated with the beeswax. SVET measurements were recorded in mapping for 96 h. SVET experiments were conducted in a flow-through cell containing 5 mL of 0.05 M NaCl electrolyte. The flow rate was set to 0.05 mL/min (controlled by a peristaltic pump Medorex TL15E), implying that the electrolyte in the cell was fully renewed every 1.5 h).

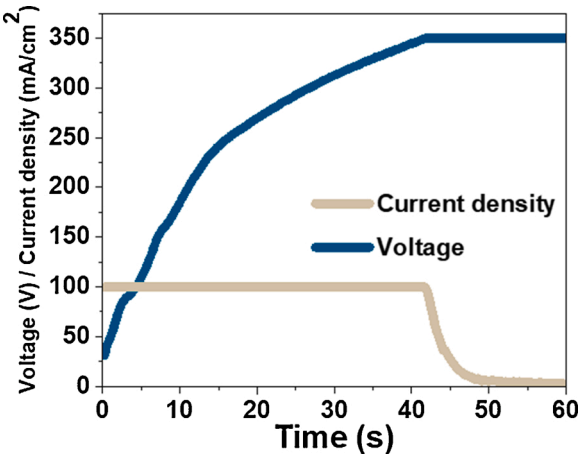

Fig. 1. The current density/voltage – time characteristics of the flash-PEO process.

The electrolyte flow in mandatory to avoid the effect of electrolyte evaporation on the conductivity/current density values [32].

A commercial SVET-SIET equipment produced by Applicable Electronics and controlled by LV4 software (Science Wares) was employed. An insulated Pt-Ir microelectrode (Microprobes Inc.) vibrated in the horizontal (X) and vertical (Z) planes relative to the surface with amplitudes of 17 μm. The vibration frequencies of the probe were 128 Hz (X) and 325 Hz (Z). The diameter of the platinum black ball was 17 ± 3 μm. The probe was positioned 100 ± 5 μm above the sample surface. All the SVET measurements were conducted in a Faraday cage in an air-conditioned lab at temperature of 21 ± 2 °C.

The NSST was carried out in accordance with the ASTM B117 standard in a 5% NaCl fog. Type of samples and tests conditions are summarized in Table 1. In case of painted samples, the coupons were masked at the bottom and edges, their surface was cross-scratched before the test according to ASTM B117 standard with a certificated tool (ISO 17872) with 0.5 mm tungsten carbide tip. The 1.5 cm scratch was made in the center of 40 × 40 mm specimens, a 50 × 50 mm cross was scribed in the

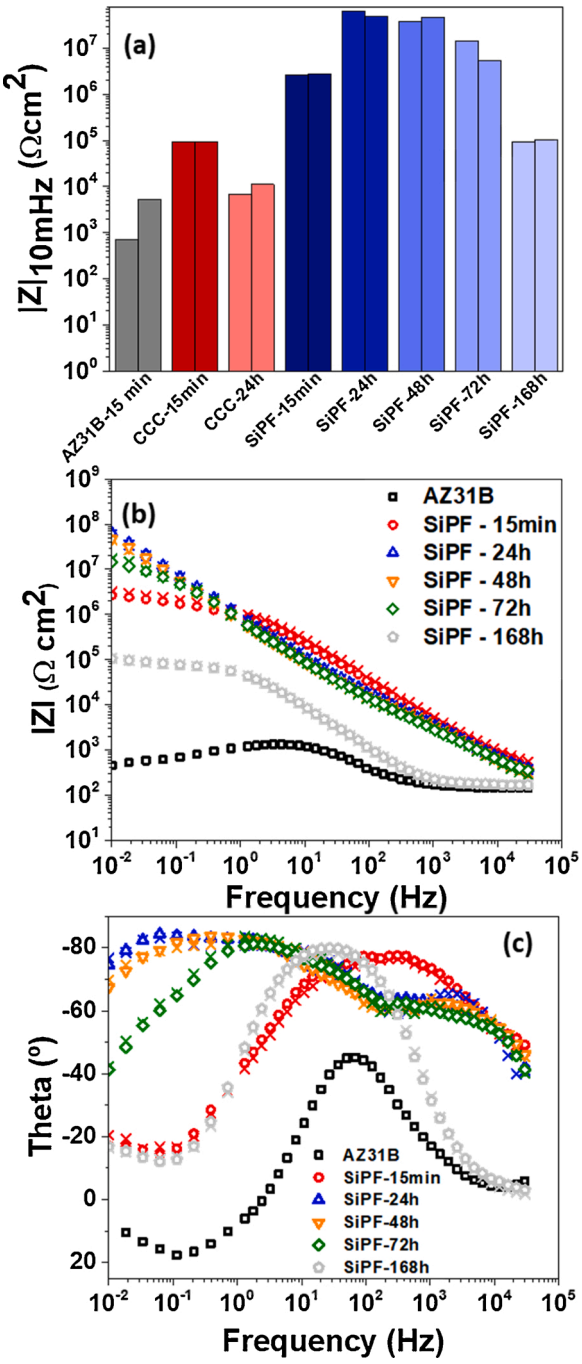

Fig. 2. (a) Total impedance modulus at 10 mHz for AZ31B substrate, CCC and SiPF coating after varied times of immersion in 0.5 % NaCl, showing repeated measurements on two different samples for each time point; (b, c) Bode plots and fitted simulated with equivalent circuit. Empty symbols correspond to the experimental data; cross symbols correspond to the fitting.

center of 75 × 250 mm coupons. Samples rating was defined according to ASTM D1654 standard. The corroded surface area of the specimens was measured by image analysis (ImageJ software) after gentle removal of the corrosion products with abrasive paper P1200 grit. The corroded distance was defined as "one sided" scribe creepage, that is from the original scribe line to the creepage front. For all salt spray tests, triplicate samples were used.

Paintability tests were carried out in accordance with EN ISO 2409 by 6 line cross-cut with 1 mm spacing applied using certified tools dedicated for this test. For dry paint adhesion test, flash-PEO-coated 40 × 40 mm specimens were painted: (i) right after, (ii) 7 days after or (iii) 10 weeks after flash-PEO treatment, cured and tested in the same day. Moreover, paint adhesion was verified after the coatings storage in aqueous environment. For this purpose, the specimens were flash-PEO-coated, painted, cured on the same day and (i) immersed in tap water for two weeks. Additionally, inhibitor-free and inhibitor-loaded and painted flash-PEO coated specimens (i.e., full system protection) were tested for paint adhesion following 2000 h of NSST. All paint adhesion tests were repeated on three specimens and the rating was calculated as an average result.

3. Results and discussion

3.1. Electrical response of flash-PEO

Fig. 1 shows time dependencies of registered current density and voltage signals during flash-PEO process in SiPF electrolyte. To ensure as low as possible energy consumption while maintaining a uniform coating appearance and thickness, the process parameters were optimized in previous experiments by variation of the treatment time and limiting voltage (60−90 s and 350−400 V, respectively). The limiting voltage of 350 V was reached after 40 s of the process and was followed by a drop in current density; micro-discharges that initiated at ~15 s (~250 V) extinguished once the current density dropped <20 mA/cm^2. The obtained coating had a uniform appearance and the thickness of 5.0 ± 0.64 μm. The resultant energy consumption was calculated to be ~4.6 kW h m^{-2} (0.95 kW h m^{-2} μm^{-1}).

3.2. EIS response of flash-PEO

The Bode EIS spectra and evolution of impedance modulus at 10 mHz with time during preliminary corrosion performance evaluation of the flash-PEO-coated and bare Mg AZ31B alloy following the immersion in 0.5 % NaCl solution for 15 min, 24 h, 48 h, 72 h and 168 h are given in Fig. 2**(a–c)** and show good repeatability. Respective Nyquist plots are presented in **Supplementary** Fig. 2. Following 15 min immersion, a significantly higher value of impedance modulus $|Z|_{10mHz}$ (Fig. 2**(a)**) (three orders of magnitude) for the flash-PEO coating compared with that of non-coated alloy indicates a much greater initial corrosion resistance of the former. Remarkably, SiPF coaing shows over ten times increase in low frequency impedance during 24 h of immersion in the corrosive medium and maintains it for up to 3 days. For comparison, a ~10 μm-thick commercial CCC used as a reference in this study (coating microstructure presented in Fig. 3**(A)** and macrograph Fig. 3**(B)**) shows about 30 times lower values after 15 min and an order of magnitude drop in $|Z|_{10mHz}$ to 10^4 Ω cm^2 following 24 h of immersion (Fig. 2**(a) and 3(C) and Supplementary** Fig. 3). For SiPF flash-PEO coating, a drop in $|Z|_{10mHz}$ below the initial value is observed after one week of immersion, however the performance is still about two orders of magnitude greater than that for the bare substrate after 15 min of immersion.

Different features of the coating are revealed depending on the immersion time. For up to 72 h of immersion, two relaxation processes are observed (Fig. 2**(b,c)**): these correspond to the response of the outer porous part of the oxide layer (at high-medium frequencies) and the intact inner barrier (at low frequencies). Further immersion in NaCl solution (168 h) allows for the migration of corrosive species through the outer layer towards the inner layer resulting in the initiation of substrate corrosion process. The corrosion processes can be described by the double layer capacitance of the electrolyte/metal interface and the polarization resistance. After this immersion time, the response of the outer porous layer has almost disappeared due to the penetration of the electrolyte; the inner barrier layer provides the main response of the system. The non-coated alloy after 15 min of immersion was also analyzed in order to be compared with the coated specimen. The distinct feature of impedance response in this case is a pseudo-inductive behavior at low frequencies, which can be explained by an apparent

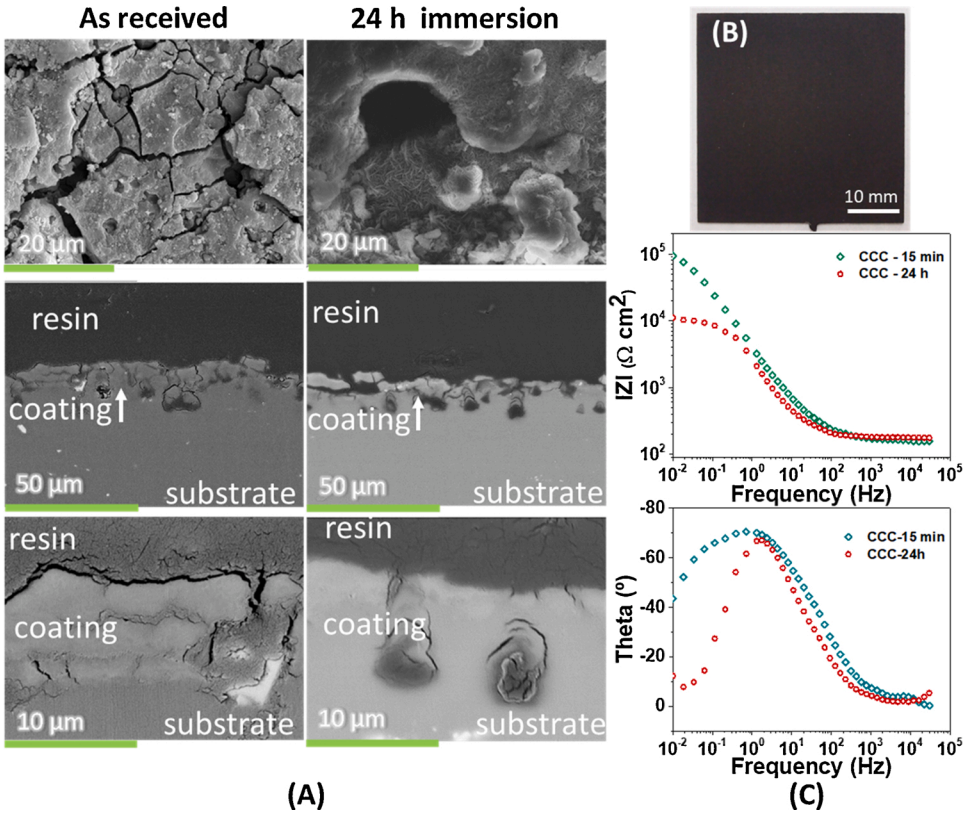

Fig. 3. (A) Secondary electron micrographs of the CCC top views (top row) and backscattered electron micrographs of CCC cross sections before and after 24 h immersion in 0.5 % NaCl and EIS measurement. (B) Macrograph of the as-received CCC surface appearance with an intense pitch-black colour. (C) Bode EIS plots for CCC after 15 min and 24 h of immersion in 0.5 % NaCl.

non-stationarity during the spectra acquisition. The low reproducibility of $|Z|_{10mHz}$ (Fig. 2**(a)**) additionally confirms this assumption. The main well defined time constant in this case can be associated to the response of the native thin oxide film present on the metal surface.

Equivalent circuits were used to fit the experimental data of the coated specimens (Fig. 4**(a)**). They include R_s that accounts for the resistance of the electrolyte and Constant Phase Elements (CPE) that account for non-ideal capacitive behavior of the system. The Constant Phase Elements (CPE) account for non-ideal capacitive behavior of the system due to different phenomena (non-uniform region, inhomogeneous reaction rates on the surface varying thickness or composition of a coating and/or non-uniform current distribution) [33–35]. The impedance of a constant phase element is described as (Eq. 1):

$$Z_{CPE} = \frac{1}{T(j\omega)^n} \quad (1)$$

where T is the CPE constant, which nominally equals to admittance of the system at 1 rad/s; $j = \sqrt{-1}$, ω is the angular frequency (rad/s) and the value of n ranges between 0 and 1. If $n = 1$, CPE becomes the impedance of a pure capacitor; if $n = 0$, CPE acts as a pure resistor.

For flash-PEO coating, the CPE_{out}/R_{out} and CPE_{in}/R_{in} elements (top circuit, Fig. 4**(a)**) represent capacitive and resistive behavior of the outer porous and inner barrier layer, respectively. After 1 week of immersion (second circuit, Fig. 4**(a)**), the protective properties of the outer layer strongly decreased and the response of the electrochemical activities of the substrate appeared; hence, the CPE_{out}/R_{out} were removed and CPE_{dl}/R_{polar} were included. The latter two elements are associated with the double layer capacitance on the electrolyte/metal interface and the polarization resistance [36].

The corresponding electrochemical parameters of the equivalent circuits used to fit the experimental data are presented in Table 2. The degradation behaviour of the coating can be surmised from the evolution of R_{out}, R_{in} which are presented in Figs. 4**(b,c).** It is evident that there is a continuous decrease of the resistance ascribed to the outer part of the coating so that after one week of immersion its contribution becomes invisible. This behavior is very common for PEO coatings and is associated with their chemical degradation due to the penetration of the electrolyte through cracks and pores of the oxide layer. Regarding the inner layer resistance, an unusual initial increase is observed after 24 h of immersions; the reasons for that will be further discussed in section 3.3. The later decrease of the inner resistance with immersion time is associated with degradation of the barrier layer. After 1 week the response of the double electric layer at metal/electrolyte interface appears, meaning that the barrier layer has been breached at some locations.

3.3. Coating characterization

In order to further elucidate the corrosion protection mecanism outlined in the EIS study, the coating morphology, composition and microstructure were characterized following the different immersion times and EIS measurements. The ~5-µm-thick as-received SiPF coating shows a typical porous surface morphology (Fig. 5) with a thick outer porous layer and a thin barrier layer adjacent to the substrate. Apart from the pores that are remnants of penetrating discharge channels, the outer layer features so called pore band just above the barrier layer. This

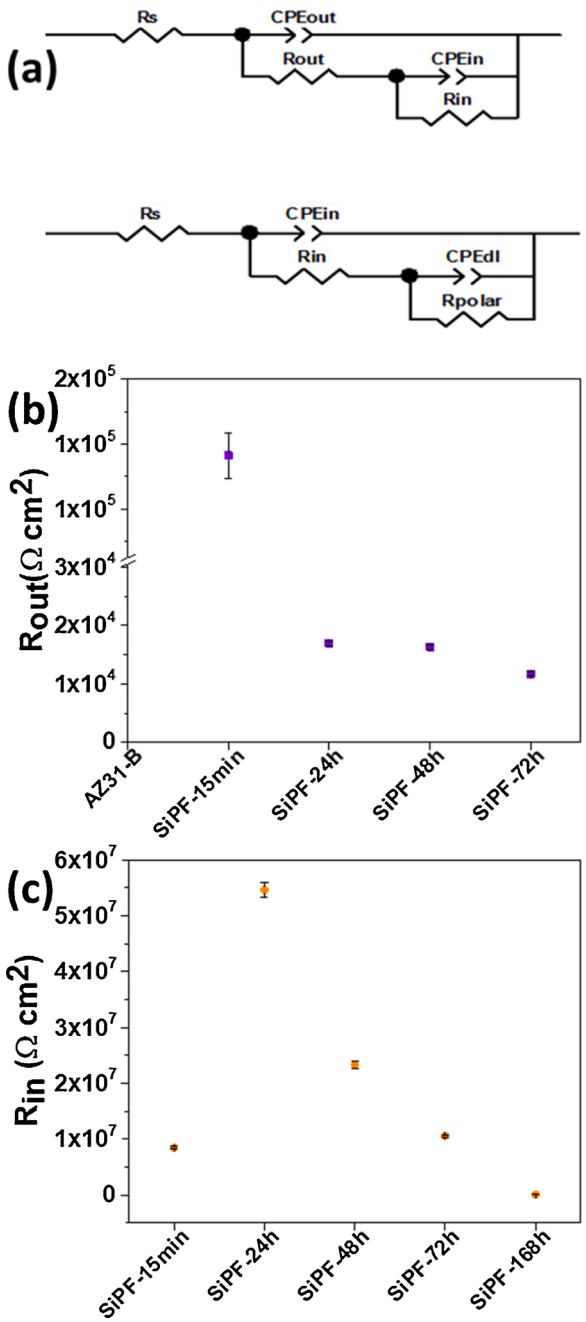

Fig. 4. (a) The equivalent electrical circuits used to fit the EIS spectra and (b) the evolution of outer layer resistance, (c) inner layer resistance during immersion in 0.5 % NaCl for up to 168 h.

band is typical for DC and unipolar pulsed DC PEO coatings on Mg but is also often observed in Al alloys under unipolar pulsed DC and pulsed bipolar PEO modes [37,38]. This band seems to be pertinent to dilute electrolytes; the pores size in the band is known to decrease as the uniformity of current distribution increases with greater interelectrode distance [39]. Ultimately, it appears to be related to temperature gradient inside the discharge channel. Current regimes that generate discharges with non-uniform temperature in the outer and inner parts of the discharge channels lead to solidification of the molten oxide ejected from the inner regions of the channel. Thus forms a surface "crust" over the area that still contains soft coating material, which is pushed and deformed by the gas under high pressure inside the channel. This pore band is never observed under so-called "soft sparking" regimes. This is possibly associated with the contraction of positive column of the

Table 2
EIS fitted data of flash-PEO coated AZ31B alloy following immersion in 0.5 wt.% NaCl. (R given in Ω cm^2; CPE given in S s^{-n} cm^{-2}).

Coating	R_s	CPE_{out}	n_{out}	R_{out}	CPE_{in}	n_{in}	R_{in}
SiPF-15 min	264.6	1.29×10^{-7}	0.84	138,220	9.23×10^{-7}	0.45	8.462×10^{6}
SiPF-24 h	262.7	1.15×10^{-7}	0.87	16,996	8.75×10^{-8}	0.93	5.46×10^{7}
SiPF-48 h	211.9	1.41×10^{-7}	0.86	16,352	1.14×10^{-7}	0.95	2.33×10^{7}
SiPF-72 h	204.5	1.11×10^{-7}	0.82	11,671	1.03×10^{-7}	0.91	1.06×10^{7}
Coating	**R_s**	**CPE_{in}**	**n_{in}**	**R_{in}**	**CPE_{dl}**	**n_{dl}**	**R_{polar}**
SiPF-168 h	171.3	2.32×10^{-6}	0.93	72,511	1.11×10^{-4}	0.65	1.01×10^{5}

microdischarge that extends through the entire coating thickness [40, 41].

Particularly interesting is the notable lack of pitting or undercoating corrosion, even after 168 h of immersion (Fig. 5 **(C, D)** rows, and **Supplementary** Fig. 4), although, corrosion manifests as progressive surface cracking. The absence of notable substrate corrosion may be due to sealing of the newly formed surface cracks and voids of the pore band during first 72 h of immersion and resistance of the thick barrier layer during the following 72−168 h. It is evident that the coating is getting progressively hydrated with time, but the barrier layer blocks the further progress of corrosion (Fig. 5 **(D),** 7 days). This corroborates the self-sealing properties of the SiPF suggested by EIS observations. Self-sealing is most likely related to two factors: i) in the small volume of the pore band the pH easily rises to the values where $Mg(OH)_2$ is stable (pH > 10.5), as Lu et al. have pointed out [42]; ii) formation of other phases in the coating which will be further discussed.

Surface roughness of the coating was evaluated by optical profilometry before and after EIS measurements following 24−72 h of immersion in 0.5 % NaCl (**Supplementary** Table 2**)**. Interestingly, roughness of the coating (as expressed by maximum valleys depth and ten point height of selected area, S_v and S_{10z}, respectively) decrease with immersion time. This is most likely related to plugging of the coating pores due to the self-sealing, i.e. the accommodation of the greater volume (resulting from coating material hydration) in the internal voids.

Cross-sectional elemental mapping (Fig. 6) confirmed an intensive incorporation of electrolyte species, particularly of silicon, into the coating during flash-PEO process; a gradient distribution of O, P, and Si (decreasing inwards) is apparent. On the contrary, F is mainly located in the inner region of the coating, since fluoride ions migrate faster in the oxide material under the electric field than oxygen. Area and point Energy Dispersive X-ray Spectroscopy (EDS) analyses were also performed on the coating surface and cross-sections following different times of immersion in 0.5 % NaCl (Fig. 7).

The decreasing trend of the evolution of selected element ratios (obtained from area analysis of the coating surface) suggests gradual coating hydration/dissolution with immersion time (Fig. 7**(a)**). Evolution of elemental content throughout coating cross-section with time shows depletion of Mg and Si in the top region and enrichment in the bottom (Fig. 7**(b,d)**). The decreasing Si/Mg and increasing P/Mg ratios (Fig. 7**(a)**) suggest that leaching of Si from a thin superficial coating layer during immersion must be proceeding more readily than dissolution of MgO and leaching of P (e.g. solubility of SiO_2 in water is rather high, 0.12 g L^{-1}, compared with An increase of O (Fig. 7**c**) is consistent with coating hydration process. A loss of F with time is particularly noticeable in the inner region of the coating (Fig. 7**(e)**), whereas P content increases with immersion both in the outer and inner regions. On the one hand, leaching of F would result in observed rise of Mg, Si and P levels (given the semi-quantitative nature of EDS) in the inner regions of the coating (Figs. 7**(b, d, f)**). Although fluoride release was not measured in this study, it is a well-known phenomenon in F-

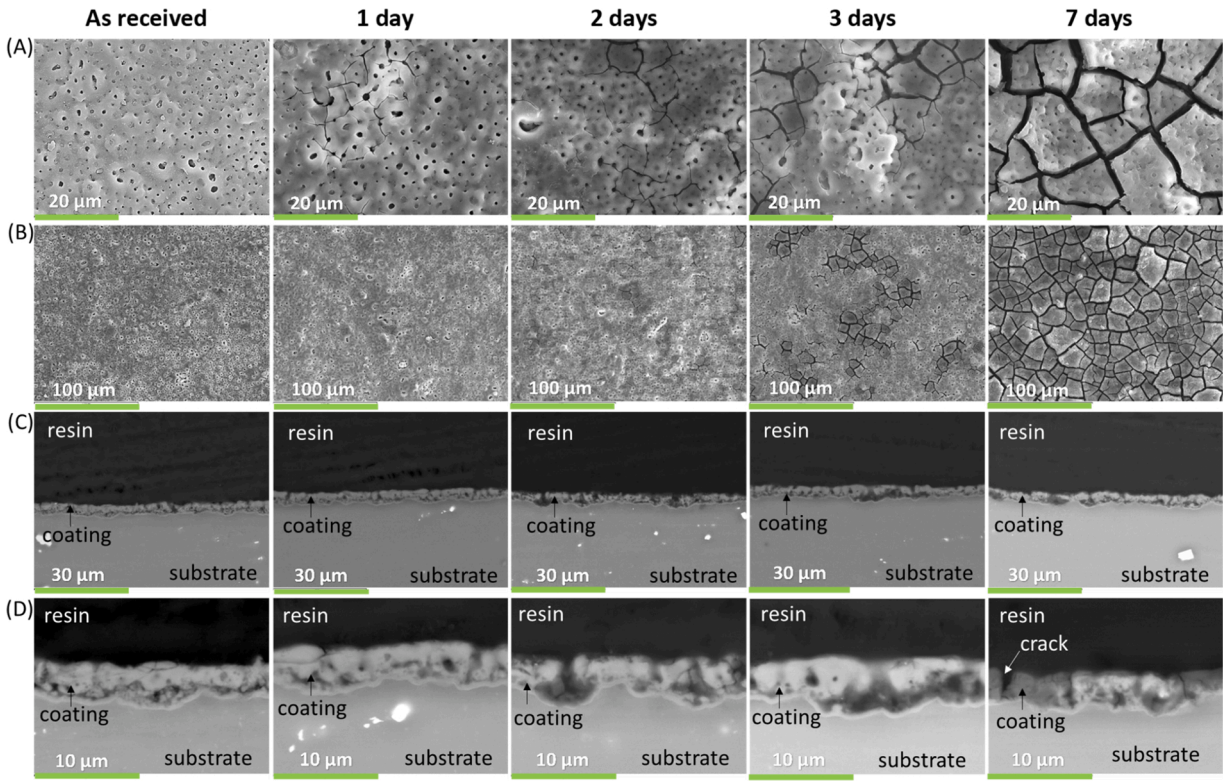

Fig. 5. Secondary electron micrographs of plan views (A, B rows) and backscattered electron cross sectional micrographs (C, D rows) of SiPF coating before and after immersion in 0.5 % NaCl and EIS measurement.

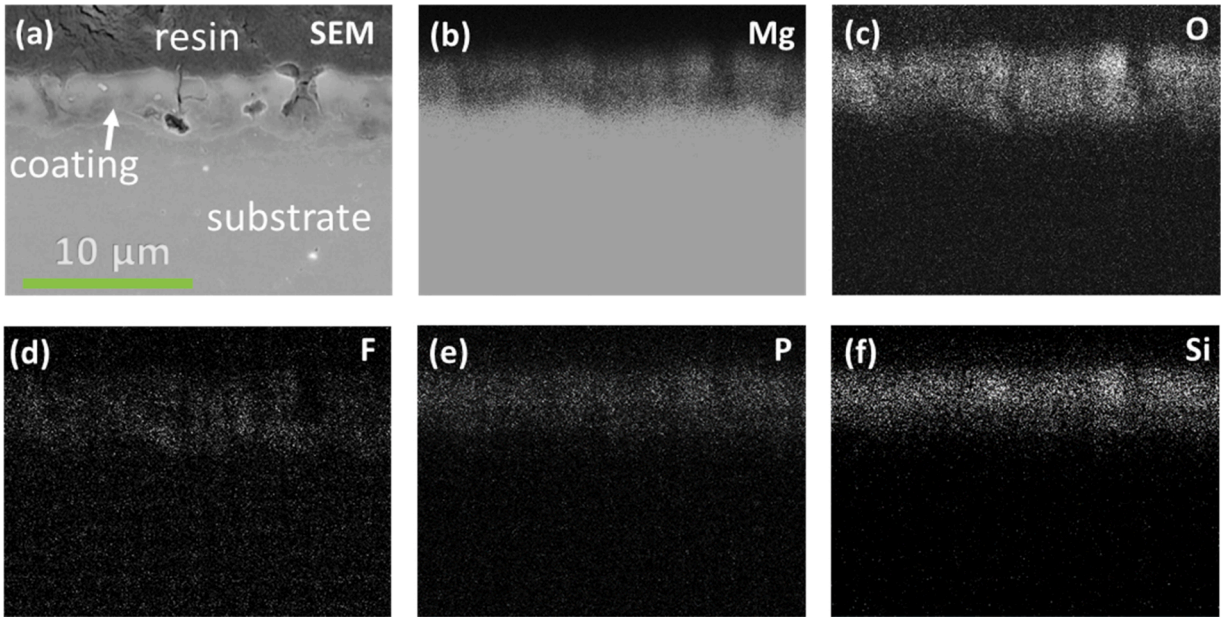

Fig. 6. (a) SEM image of the SiPF coating as-received cross-section and EDS mapping of the (b) Mg, (c) O, (d) F, (e) P, (f) Si elements.

containing PEO coatings on Mg reported by the authors previously [43, 44]. On the other hand, elevated Si and P content in the inner region of the coating and within the clogged pores (i.e. in the hydrated regions) with immersion time can be associated with a rather slow dissolution rate of Si- and P-containing amorphous phase and its participation in the self-sealing mechanism of the pore band.

Bragg-Brentano X-ray diffraction performed on SiPF coatings before and after 168 h of immersion in 0.5 % NaCl (Fig. 8**(a)**) disclosed the presence of MgO, MgF_2, $MgSiO_3$, Mg substrate as well as some unidentified Al-Mn intermetallics (at 15−20° 2θ) and amorphous material in both cases. Grazing angle X-ray diffraction patterns (Fig. 8**(b)**) revealed that the coating surface contained only MgO in the as received state and completely amorphous coating material after immersion (Mg peaks present in both specimens appear because the specimens were coated only on one side but not on the edges). These findings, in combination with Bragg-Brentano patterns and EDS mapping (Fig. 6), suggest that

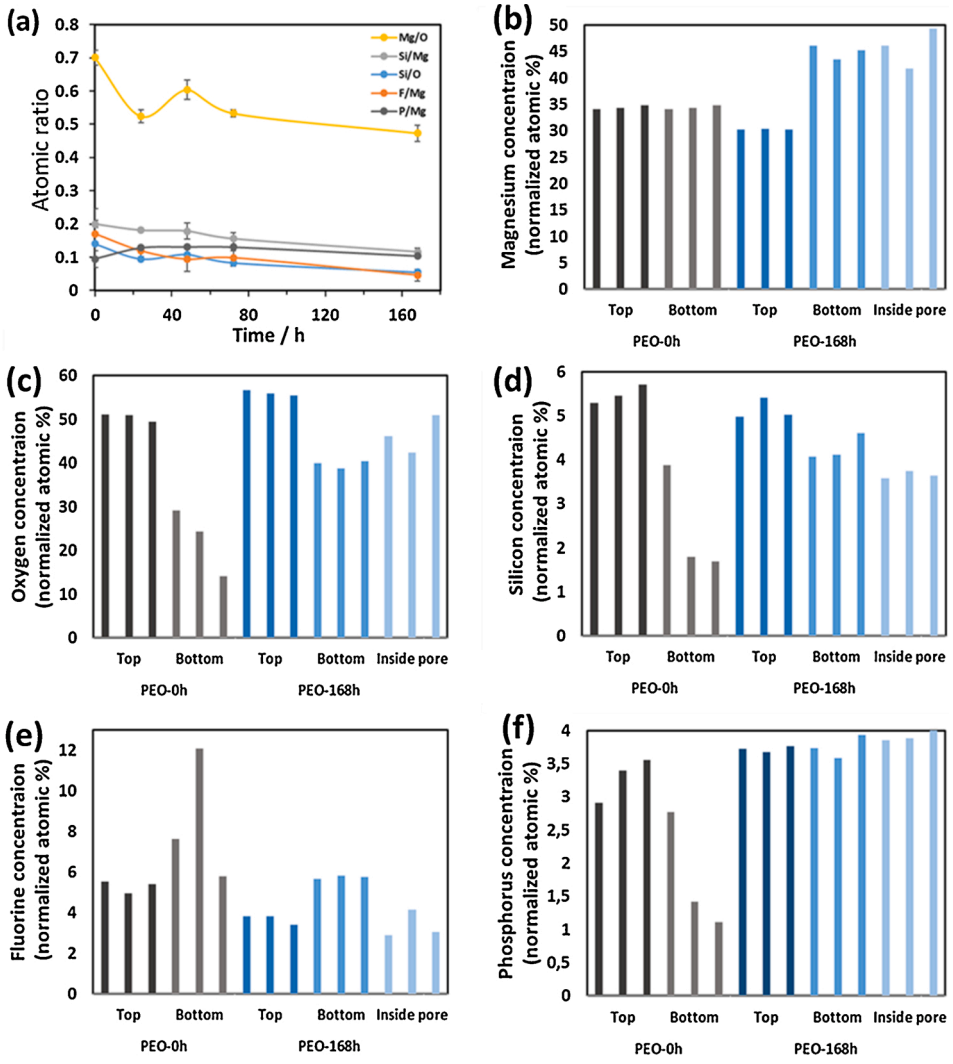

Fig. 7. EDS analysis of the SiPF coating: (a) evolution of surface elemental ratios with immersion time in 0.5 wt.% NaCl; (b-f) variation of elemental content in different regions of the coating in as received conditions and following the immersion in in 0.5 wt.% NaCl for 168 h.

crystalline MgF_2 and $MgSiO_3$ are mainly located in the inner regions of the coating, whereas the top part of the coating surface (probed by grazing incident angle) contains crystalline MgO and amorphous F-, Si- and P-rich phases. Disappearance of MgO peaks in the surface following immersion can be explained by coating hydration and formation of amorphous $Mg(OH)_2$ which is typical for corrosion of PEO coatings on Mg alloys.

Bragg-Brentano diffractograms (Fig. 8**(a)**) suggest dissolution of $MgSiO_3$ from the inner regions of the coating as evidenced by the decrease of its corresponding diffraction peak at 43.7°, whereas MgF_2 preserves its crystallinity after the immersion.

Further development of the protection system involved impregnation of the flash-PEO coating with organic inhibitors. Previously, a group of organic inhibitors were tested on bare alloy. Fig. 9**(a)** shows the evolved H_2 during the immersion for 3 days. As can be seen, presence all the tested inhibitors in the reference electrolyte (0.5 wt. % NaCl) leads to lower evolved H_2 after 3 days of immersion, showing their effectiveness in the reduction of AZ31 corrosion rate. However, a few of the inhibitors are not able to inhibit the corrosion within the first few hours of immersion; specifically, DBS-Na can accelerate the corrosion of the bare AZ31 within the first day of immersion.

Based on the results of the H_2 evolution tests, the inhibition efficiency (IE) of each inhibitor was calculated by the following Eq. 2:

$$IE(\%) = \frac{V_{ref} - V_{inh}}{V_{ref}} \times 100\% \quad (2)$$

Where V_{ref} and V_{inh} are the amounts of H_2 (ml) evolved at a certain time of immersion in the reference solution (NaCl 0.5 wt. %) and in the solution containing corrosion inhibitors. Both IE obtained at 20 h and 70 h of immersion were taken into account for choosing the best-performing inhibitors to be incorporated into the PEO coating (Fig. 9**(b)**). The selected best-performing inhibitors are 4Methylsalicylate-Na, 3Methyl2Nitrobenzoate-Na, Quinaldate-Na, and 2,5PDC-Na.

These were incorporated into the PEO and their effect on the corrosion protection properties of the coated system was evaluated through the NSST of painted and scribed specimens (Fig. 10). Note that the results shown in Fig. 10 are the more severe corrosion creepage observed out of two repetitions for each impregnated inhibitor. The corrosion creepage initiates from separate points of the scribe and its propagation is similar to the common filiform corrosion of the coated magnesium. As an example of filiform corroded area appearance, SiPF sample stereomicroscope image is presented in **Supplementary** Fig. 5. The visual comparison of the macrographs in Fig. 10 reveals that for the incorporated inhibitors 2,5PDC-Na, 3Methyl2Nitrobenzaote-Na, and Quinaldate-Na, there is no remarkable difference in corrosion creepage extension after 7 days of NSST. However, the sample loaded with

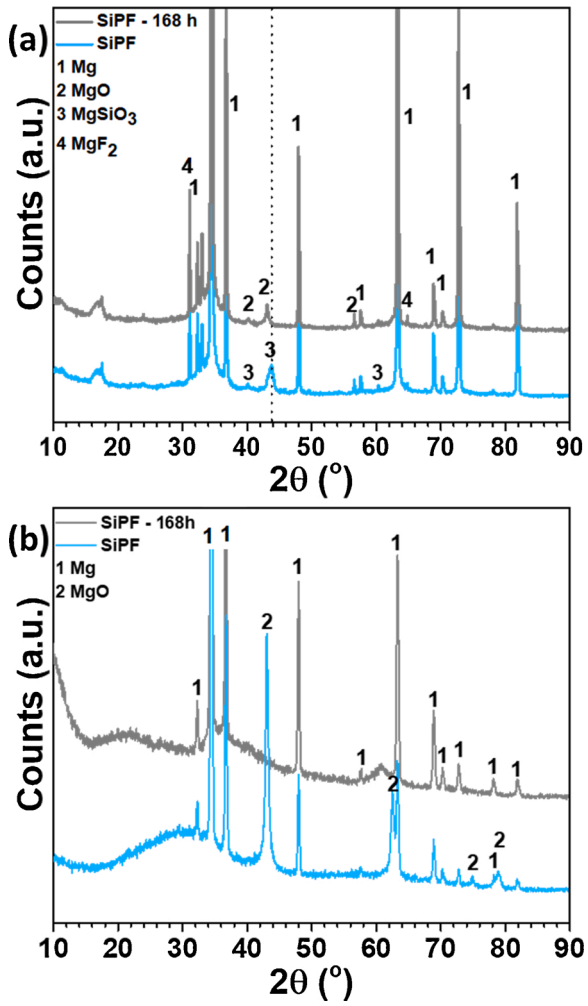

Fig. 8. (a) Bragg-Brentano and (b) grazing angle X-ray diffractograms of SiPF PEO coating as received and after 168 h of immersion in 0.5 % NaCl.

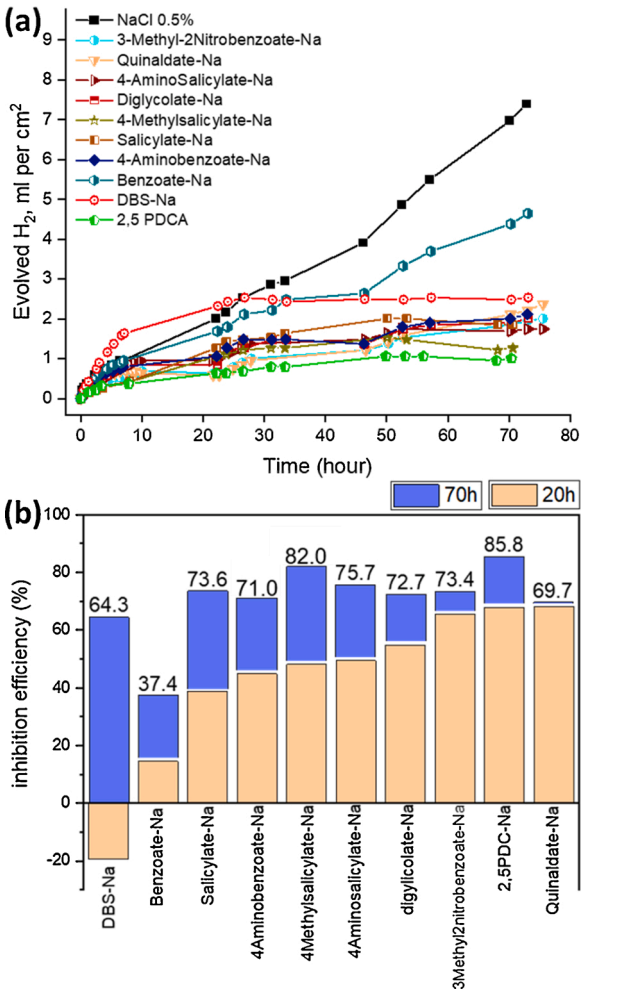

Fig. 9. (a) Normalized H_2 evolution on AZ31B alloy immersed in 0.5 wt. % NaCl in the presence of inhibitors. Initial pH of all the tested electrolytes was close to neutral (6.8-7.2). (b) Inhibition efficiency calculated after 20 h and 70 h of H_2 evolution test. The numbers on top of each column are IE after 70 h.

4Methylsalicylate (4MSA) lasts with no observable creepage to the sides of the scribe after 7 days of NSST. Therefore, the PEO-coated AZ31 impregnated with 4MSA was chosen as the best-performing inhibitor to impede the corrosion of PEO coated AZ31, and thus, subjected to further investigation.

ATR FTIR analysis of the SiPF and SiPF/4MSA coatings did not reveal any significant differences between the coatings (Fig. 11). In general, the rough porous morphology of the PEO coatings makes FTIR analysis difficult. However, some important corroborations were obtained in regards to the presence of the electrolyte species responsible for self-sealing behaviour of the coatings. Features commonly found in hydrated metal oxides and PEO coatings included a broad band between 3500 cm^{-1} and 3300 cm^{-1} ascribed to stretching mode of −OH groups; a small band around 1630 cm^{-1} related to bending of H–O–H and a peak at the lowest wavenumbers (inset, Fig. 11) around 400−546 cm^{-1} assigned to stretching vibrations of Mg-O and Mg-F bonds [45]. A small peak at 1430 cm^{-1} is likely to be associated with carbonates as a result of the reaction of hydroxylated MgO with CO_2 from the atmosphere [46]. Finally, the prominent broad peak at 941 cm^{-1} can be ascribed to overlapping of responses from several species. $P_2O_7^{4-}$ is known to be manifested at around 941 cm^{-1} and 846 cm^{-1}; 932 cm^{-1} and 937 cm^{-1} are ascribed to stretching of Si-O bonds in SiO_3^{2-} [47,48]. In the presence of Mg cations silica tetrahedra may contain two or three non-bridging oxygen atoms, i.e. they are depolymerized. The shoulder that can be discerned at around 1042 cm^{-1} (inset, Fig. 11) is likely to be a further manifestation of asymmetric Si–O stretching. Thus, FTIR and MicroFTIR results largely support the hypothesis that Si- and P-containing phases participate in coating self-sealing mechanism.

3.4. Local electrochemical characterization

The set of current density maps, each accompanied by corresponding optical micrograph is shown in Fig. 12. Three samples have been immersed in 0.05 M NaCl solution for four full days: CCC treated, flash-PEO treated SiPF and flash-PEO impregnated with the corrosion inhibitor, SiPF-4MSA. While the set of SVET maps with optical micrographs (Fig. 12) shows the representative snapshots, the evolution of the peak current density presented in Fig. 13 directly reflects the magnitude of the corrosion attack and protection of each sample at any given time.

In general, for all the samples the anodic currents are characterized by higher maximum values compared to that of cathodic (by modulus), suggesting highly localized character of the corrosion process (pitting and filiform). The time-lapse videos of the surface appearance covering 94 h of immersion are presented as Supplementary Data (**Link**). Several

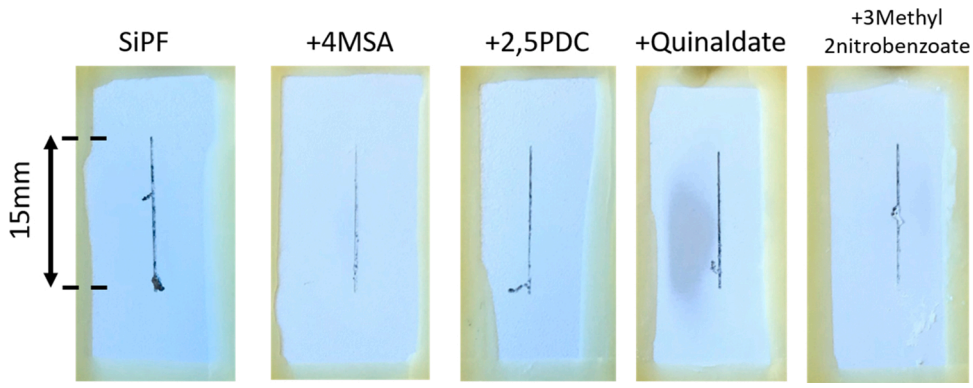

Fig. 10. Macrographs of the SiPF coatings without inhibitor and with 4 different incorporated inhibitors after 7 days of SST. All samples were painted similarly.

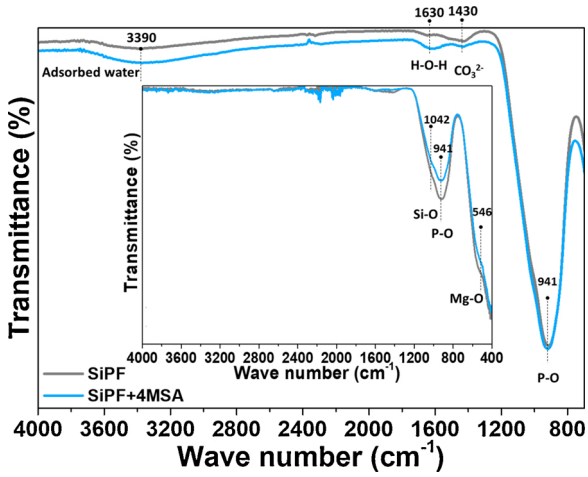

Fig. 11. ATR MicroFTIR spectra and ATR FTIR spectra (inset) of the flash-PEO coating with and without 4MSA inhibitor in the as-received state.
Fig. 12 Continued.

distinct characteristics of each coating can be underlined. The industrial reference, CCC-treated sample was rather active in terms of corrosion outbreaks from the first day of immersion. Some active centers, that can be identified in SVET maps and as hydrogen bubbles in optical micrographs and time-lapse video, were persistently active throughout the immersion test, while corrosion activity in other active spots ceased and other areas of the sample became corrosively active.

Corrosion activity in both types of PEO treated sample did not start before the third day of immersion, which suggests its strong barrier effect. However, once corrosion activity broke down in SiPF PEO sample, it proceeded with the local current density 4–6 times higher than that of CCC-treated sample. Barring a short break in corrosion activity at 63–65 hours of immersion, corrosion activity persisted in SiPF PEO sample, which is a typical behavior for uninhibited magnesium alloy. The time-lapse video demonstrates extensive growth of filiform corrosion after 52 h of immersion. Rapid filiform corrosion was aggravated by crevice corrosion at the interface with the insulating beeswax. The most durable corrosion protection, combining barrier and active protection was revealed by inhibitor impregnated PEO sample, SiPF - 4MSA. Corrosion activity broke down there later than in any other sample. The time-lapse video demonstrates the outbreak of filliform corrosion after 58 h of immersion but the activity in this first site ceased within one hour. Soon after that another outbreak of filiform corrosion was activated in different part of the sample. There, corrosion activity lasted at the magnitude similar to that shown by CCC coating and then decreased to minimal values. It is rather unique that the filiform corrosion in magnesium alloy was largely suppressed demonstrating the intrinsic active corrosion protection provided by the composite coating. This passive behavior continued for more than 20 h, until the end of the immersion test.

3.5. *Full system testing*

In order to reveal anticorrosive properties in simulated environmental conditions the CCC, SiPF and SiPF/4MSA-coated specimens were painted with non-inhibiting epoxy chromate-free primer, scribed and exposed for 7 days to accelerated corrosion conditions in NSST. Macrographs of the corrosion progress and rating of the creepage (Fig. 14 **(A))** reveal closely similar performance for SiPF coating and CCC. The measured corroded distance defined as “one sided” scribe creepage (that is from the original scribe line to the creepage front) gives the average rating of 8 for both CCC and SiPF samples, however the creepage from the scribe in CCC sample has extended more than SiPF sample and small blisters also can be observed on CCC sample specially around the scratch. The inhibitor-loaded SiPF/4MSA coating yielded a rating of 10 (negligible creepage). The cross-sectional examination reveals that corrosion damage is shallower for SiPF as compared to CCC. However, SiPF/4MSA has minimal visible extension of the corrosion into the substrate (Fig. 14 **(B)**). Higher magnification cross-sectional micrographs disclose good adhesion of flash-PEO coating to the substrate at the edge of the scratch (Fig. 14 **(C)**) and excellent paint adhesion to the coatings in the locations further away from the scratch (Fig. 14 **(D)**). **Supplementary** Fig. 6 further discloses that inhibitor-free non-painted SiPF coating shows minimal corrosion after 24 h of NSST with the percentage of corroded surface area of 0.2 %, which corresponds to 9 in 10-point scale of the rating.

Paintability of SiPF and SiPF/4MSA coatings was evaluated in both dry and wet paint adhesion tests. Fig. 15 shows the results of tests on 40 × 40 mm specimens painted by draw-bar. Dry paintability was excellent (rating 0) on both freshly prepared and 10 week-aged (stored in a dessicator) SiPF coatings. These results were undoubtedly ensured by the inherent porosity of PEO coatings, advantageous for paint application. Wet paint adhesion to SiPF coating tested following two weeks of immersion in distilled water (Fig. 15 **(c)**) was equally good. Incorporation of 4MSA did not impair the paintability of SiPF flash-PEO coating, which yielded rating 0 even after 2000 h in NSST chamber (Fig. 15 **(d, e)**).

Since SiPF/4MSA coating showed an excellent active corrosion protection performance in lab-scale sized specimen, the coating process was scaled up for large size coupons typically used in industrial salt spray and paintability tests. A full system comprised a SiPF/4MSA coating in combination with either a state-of-the-art chromate-free primer with active inhibition [31] or non-inhibiting epoxy chromate-free primer. A commercial CCC combined with either chromated primer or non-inhibiting epoxy chromate-free primer was included in the testing batch for comparison. The full system was evaluated in scribed and non-scribed conditions, insulating the corners and

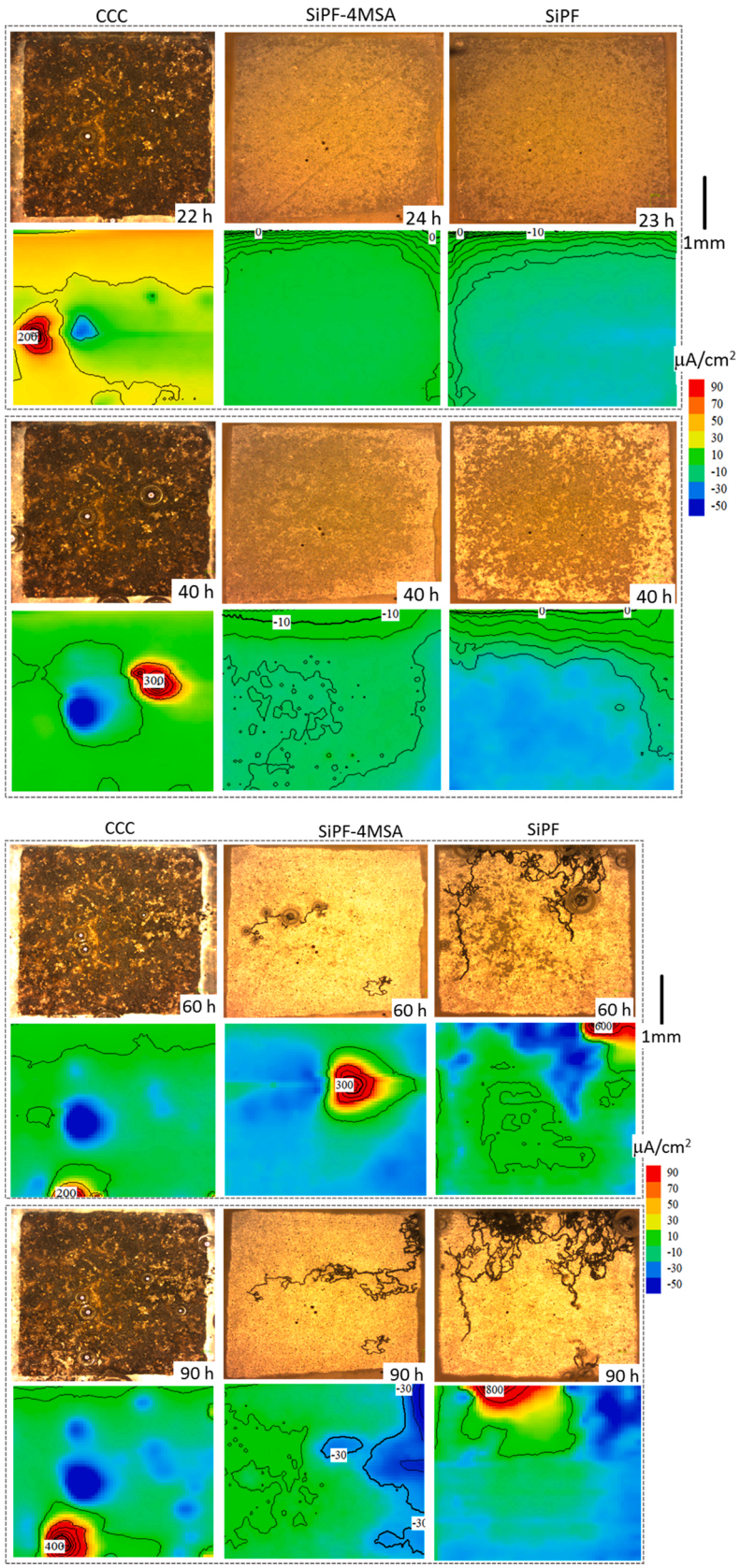

Fig. 12. Optical micropgraphs and SVET current density maps of reference CCC and SiPF coatings with and without 4MSA ihibitor aquired during immersion in 0.05 M NaCl. The immersion time is specified in each section of this Figure.

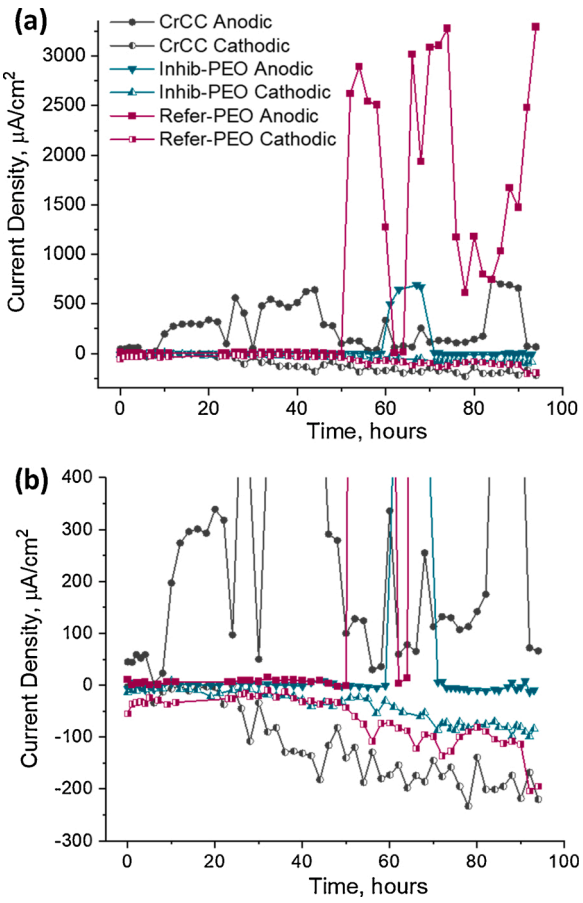

Fig. 13. Evolution of the peak current density, anodic and cathodic, for three types of tested samples during 96 h of immersion in 0.05 M NaCl.

edges of the coupons with a tape in order to protect non-uniform and bare parts of the samples, such as the electrical contact sites for PEO. Non-painted CCC and SiPF/4MSA were also included in the NSST test.

Following 24 h exposure the non-painted CCC (for better resolution see **Supplementary** Fig. 7**)** disclosed an extensive corrosion damage (Fig. 16), whereas SiPF/4MSA coating remained relatively intact; although by 168 h the latter developed numerous pits, the attack was much less severe than in case of CCC. Non-scribed painted panels with SiPF/4MSA following 1000 h of exposure disclosed damage only at the sites of electrical contact for PEO where the insulating tape leaked (the tape did not fail in every panel). In comparison, non-scribed painted CCC failed in numerous locations by pitting in case of inhibitor-free primer and in a more localized manner in case of chromated primer. In case of scribed panels, both CCC and SiPF/4MSA with non-inhibiting primer, as well as CCC with chromated primer showed initiation of corrosion creepage at 168 h; SiPF/4MSA/chromate-free primer with active inhibition system was corrosion-free at 168 h and by 1000 h developed damage only around the defect and to a much lesser extent than CCC with chromated primer.

Dry and wet paint adhesion results on large coupons are provided in Table 3. SiPF/4MSA system with either type of primer performed similarly well in comparison with CCC with chromated or inhibitor-free primer, yielding rating 0 in most of the panels. Paint adhesion to SiPF/4MSA coating practically was not affected by 1000 h exposure to NSST. Low wet paint adhesion performance of CCC with either type of paint may be related to the extended paintability window.

4. Conclusions

1 Stand-alone flash-PEO SiPF coating:

- A ~5 μm-thick DC flash-PEO coating enriched in Si and P species was successfully formed on Mg alloy in 60 s with a specific energy consumption of 0.95 kW h m^{-2} μm^{-1}.
- The coating exhibits a strong barrier property and a self-sealing capacity with a corrosion resistance increasing over 72 h of immersion in 0.5 wt.% NaCl due to clogging of coating pores with Si- and P-rich amorphous phase.
- After 24 h of NSST the coating exhibits an 0.2 % of corrosion damage compared with 9.1 % for commercial CCC.
- SiPF coating exhibits an excellent dry and wet (after 2000 h of NSST) paint adhesion, with a paintability window of up to 10 weeks.

2 4MSA-loaded flash-PEO SiPF coating:

- 4MSA inhibitor loaded into the pores of flash-PEO coating suppresses the local anodic current density by 4–6 times compared with stand-alone coating. The non-painted composite SiPF/4MSA coating system shows better corrosion performance than non-painted CCC by supressing filiform and pitting corrosion and providing active protection.

3 Full system performance:

- In combination with inhibitor-free primer, SiPF/4MSA composite coating shows better corrosion protection performance, i.e. negligible corrosion creepage, than CCC with the same primer after 168 h of NSST.
- In combination with a lithium-leaching active inhibition primer SiPF/4MSA composite coating shows better performance than CCC combined with chromate-containing primer after 1000 h of NSST of scribed panels.

- Following industrial-style primer application, SiPF/4MSA composite coating exhibits comparable or better dry and wet paint adhesion performance compared with CCC with either inhibitor-free or chromate-containing primer.

In summary, flash-PEO coatings on Mg alloys in combination with active protection organic inhibitor can be recommended for exploitation on industrial level as an equally effective corrosion protection system alternative to CCC for paint-baring and paint-free applications. In combination with a primer based on the promising lithium leaching coating technology, flash-PEO is a strong candidate as replacement of CCC and chromate-based coatings.

Data availability

The raw/processed data required to reproduce these findings cannot be shared at this time as the data also forms part of an ongoing study.

CRediT authorship contribution statement

E. Wierzbicka: Conceptualization, Data curation, Formal analysis, Investigation, Methodology, Validation, Visualization, Supervision, Writing - original draft, Writing - review & editing. **B. Vaghefinazari:** Investigation, Validation, Writing - original draft, Writing - review & editing. **S.V. Lamaka:** Investigation, Validation, Writing - original draft, Writing - review & editing, Supervision, Resources, Funding acquisition. **M.L. Zheludkevich:** Validation, Writing - original draft, Writing - review & editing. **M. Mohedano:** Validation, Writing - original draft, Writing - review & editing. **L. Moreno:** Investigation. **P. Visser:** Validation, Resources, Writing - original draft, Writing - review & editing. **A. Rodriguez:** Investigation, Validation, Project administration. **J. Velasco:** Investigation, Validation. **R. Arrabal:** Conceptualization, Resources, Software, Supervision, Writing - original draft, Writing - review & editing, Funding acquisition. **E. Matykina:** Conceptualization, Project administration, Resources, Software, Supervision, Writing - original draft, Writing - review & editing, Funding acquisition.

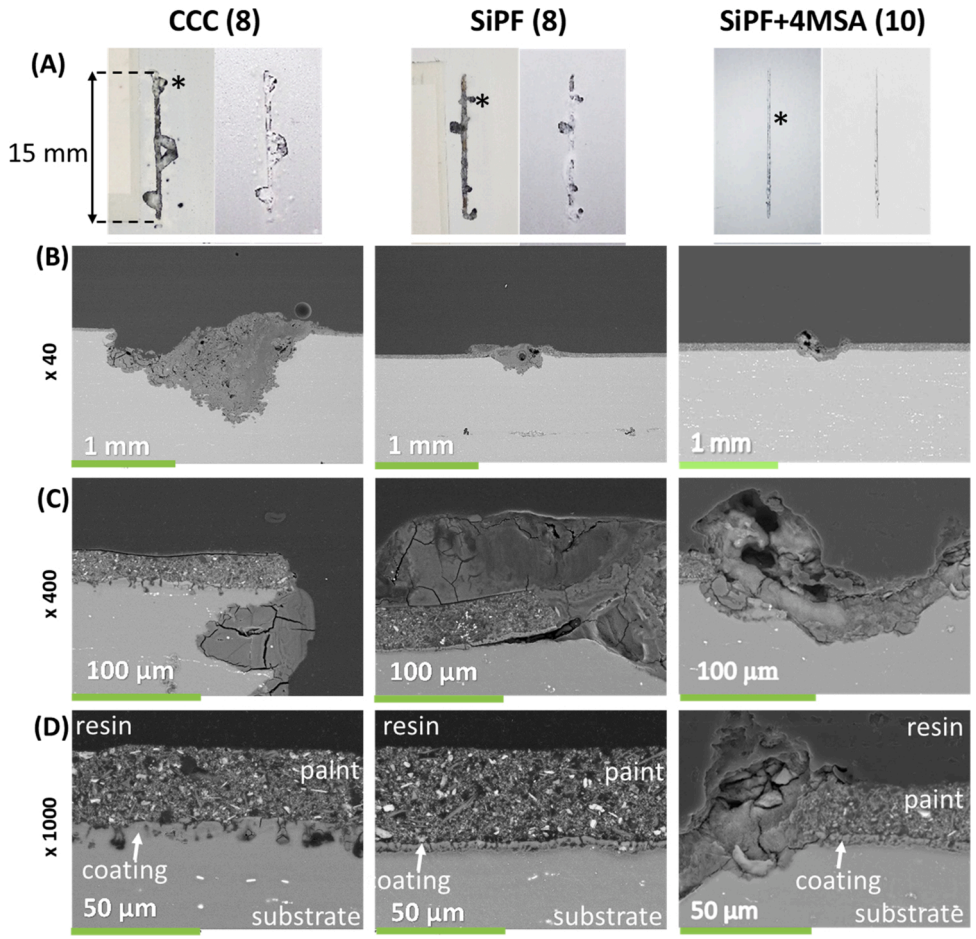

Fig. 14. A: macro photographs of the scribed area of painted specimens and average creepage after 7 d of NSST. Backscattered electron cross-sectional micrographs of the scribed area (B and C) from the places marked with an asterisk on (A) and adjacent regions that show the state of the SiPF coating and substrate under the paint (D).

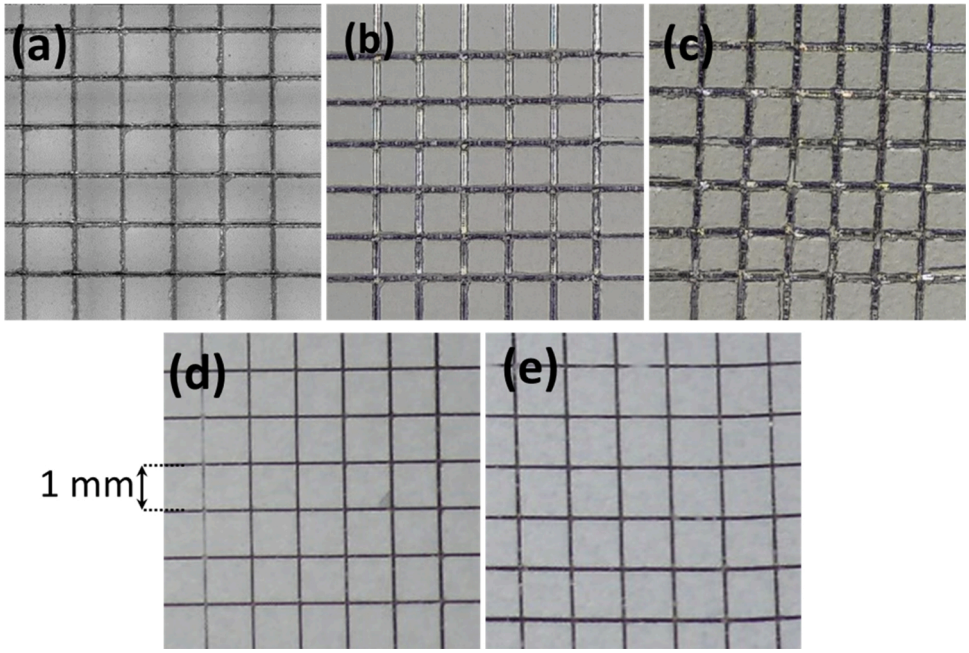

Fig. 15. Dry paint adhesion on SiPF coating: (a) same day after flash-PEO; (b) 10 weeks after PEO. Wet paint adhesion: (c) on SiPF coating after 2 weeks of immersion in water; (d) on SiPF coating after 2000 h of NSST; (e) on SiPF/4MSA coating after 2000 h of NSST. All tests are on 40 × 40 mm specimens painted by draw-bar.

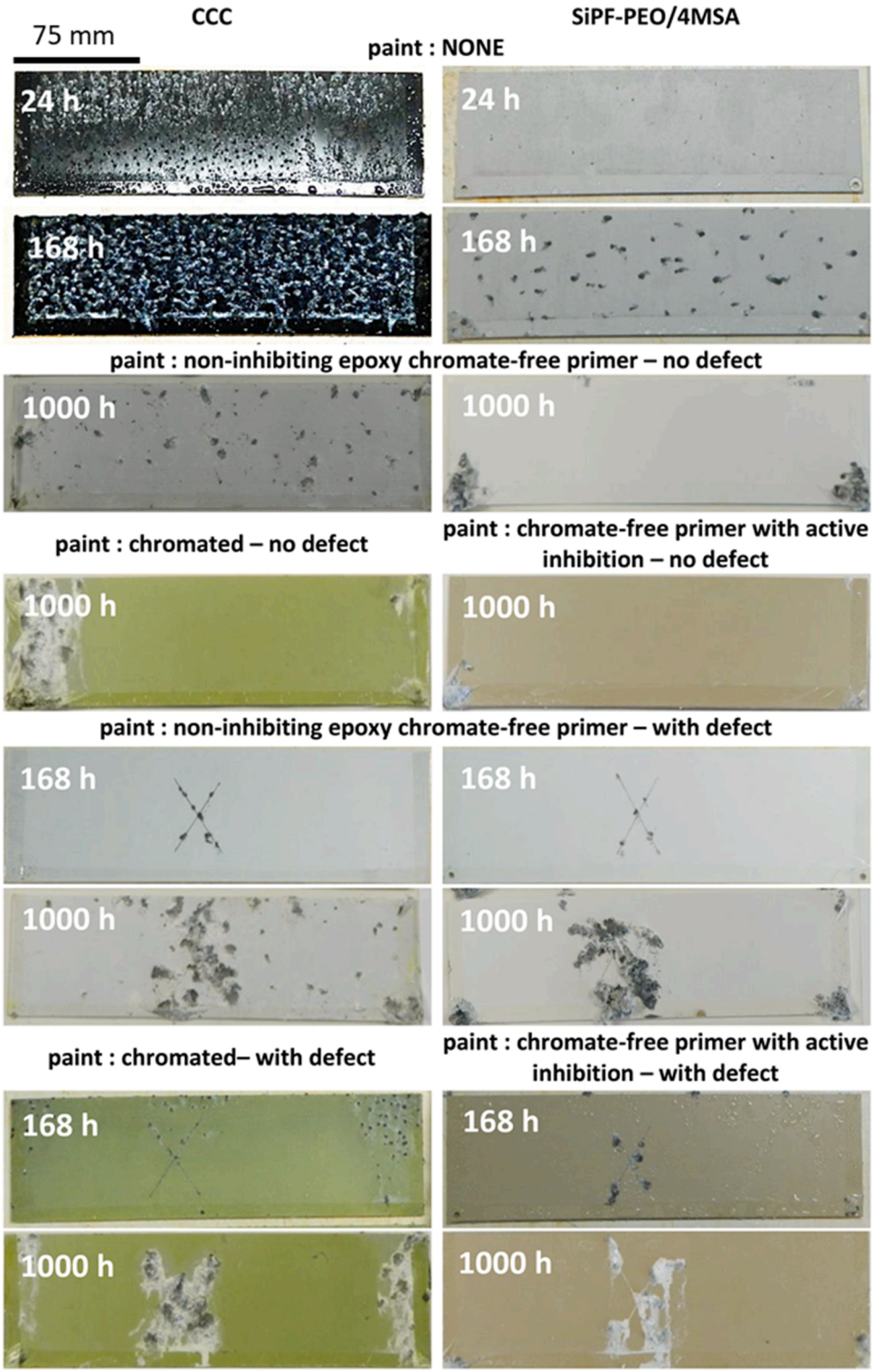

Fig. 16. NSST results for full system (SiPF/4MSA/primer) protection with and without scribed defect (in the form of a cross in the centre) in comparison with CCC/chromated primer system. The test inluded 5 panels for each system, the middle-road coupon is shown.

Table 3
Results of dry and wet paint adhesion testing of conversion coatings on AZ31B alloy carried out in accordance with EN ISO 2409.

		CCC/Primer		SiPF/4MSA/Primer	
Nº sample	Test	37,076	Chromated	No ihibition	Active inhibition
1		0	0	0	0
2		0	0	0	1
3	Dry	0	0	0	0
4		1	0	1	0
5		1	1	0	1
1		5 - 5 -3	3	0	0
2		5 - 5 -4	3	0	1
3	Wet	5	3 - 4 -4	0	0
4		5 - 4 -4	3	1	0
5		4 - 4 - 5	3 - 3 -4	1	0

Declaration of Competing Interest

The authors declare that they have no known competing financial interests or personal relationships that could have appeared to influence the work reported in this paper.

Acknowledgements

The authors gratefully acknowledge the support of the ALMAGIC project (H2020 Clean Sky 2, Grant agreement Nº 755515) and RTI2018-096391-B-C33 (MCIU/AEI/FEDER, UE). L. Moreno is grateful for the support of ADITIMAT-CM (S2018/NMT-4411). M. Mohedano is grateful for the support of RYC-2017-21843.

Appendix A. Supplementary data

Supplementary material related to this article can be found, in the online version, at doi:https://doi.org/10.1016/j.corsci.2020.109189.

References

[1] A.L. Yerokhin, X. Nie, A. Leyland, A. Matthews, S.J. Dowey, Plasma electrolysis for surface engineering, Surf. Coatings Technol. 122 (1999) 73–93, https://doi.org/10.1016/S0257-8972(99)00441-7.
[2] D. Chen, R. Wang, Z. Huang, Y. Wu, Y. Zhang, G. Wu, D. Li, C. Guo, G. Jiang, S. Yu, D. Shen, P. Nash, Evolution processes of the corrosion behavior and structural characteristics of plasma electrolytic oxidation coatings on AZ31 magnesium alloy, Appl. Surf. Sci. 434 (2018) 326–335, https://doi.org/10.1016/j.apsusc.2017.09.232.
[3] F. Monfort, A. Berkani, E. Matykina, P. Skeldon, G.E. Thompson, H. Habazaki, K. Shimizu, Development of anodic coatings on aluminium under sparking conditions in silicate electrolyte, Corros. Sci. 49 (2007) 672–693, https://doi.org/10.1016/j.corsci.2006.05.046.
[4] R. Arrabal, E. Matykina, T. Hashimoto, P. Skeldon, G.E. Thompson, Characterization of AC PEO coatings on magnesium alloys, Surf. Coatings Technol. 203 (2009) 2207–2220, https://doi.org/10.1016/j.surfcoat.2009.02.011.
[5] R. Arrabal, M. Mohedano, E. Matykina, A. Pardo, B. Mingo, M.C. Merino, Characterization and wear behaviour of PEO coatings on 6082-T6 aluminium alloy with incorporated α-Al_2O_3 particles, Surf. Coatings Technol. 269 (2015) 64–73, https://doi.org/10.1016/j.surfcoat.2014.10.048.
[6] M. Kaseem, S. Fatimah, N. Nashrah, Y.G. Ko, Recent progress in surface modification of metals coated by plasma electrolytic oxidation: principle, structure, and performance, Prog. Mater. Sci. (2020), 100735, https://doi.org/10.1016/j.pmatsci.2020.100735 in press.
[7] P. Cerchier, L. Pezzato, C. Gennari, E. Moschin, I. Moro, M. Dabalà, PEO coating containing copper: a promising anticorrosive and antifouling coating for seawater application of AA 7075, Surf. Coatings Technol. 393 (2020), 125774, https://doi.org/10.1016/j.surfcoat.2020.125774.
[8] E. Matykina, R. Arrabal, M. Mohedano, B. Mingo, J. Gonzalez, A. Pardo, M. C. Merino, Recent advances in energy efficient PEO processing of aluminium alloys, Trans. Nonferrous Met. Soc. China (English Ed. 27 (2017) 1439–1454, https://doi.org/10.1016/S1003-6326(17)60166-3.
[9] M. Mohedano, E. Matykina, R. Arrabal, B. Mingo, M.L. Zheludkevich, PEO of rheocast A356 Al alloy: energy efficiency and corrosion properties, Surf. Interface Anal. 48 (2016) 953–959, https://doi.org/10.1002/sia.5815.
[10] E. Wierzbicka, B. Pillado, M. Mohedano, R. Arrabal, E. Matykina, Calcium doped flash-peo coatings for corrosion protection of Mg alloy, Metals 10 (2020) 916, https://doi.org/10.3390/met10070916.
[11] R. del Olmo, M. Mohedano, P. Visser, E. Matykina, R. Arrabal, Flash-PEO coatings loaded with corrosion inhibitors on AA2024, Surf. Coatings Technol. 402 (2020), 126317, https://doi.org/10.1016/j.surfcoat.2020.126317.
[12] R. del Olmo, M. Mohedano, B. Mingo, R. Arrabal, E. Matykina, LDH post-treatment of flash PEO coatings, Coatings 9 (2019) 6–20, https://doi.org/10.3390/coatings9060360.
[13] C. Blawert, W. Dietzel, E. Ghali, G. Song, Anodizing treatments for magnesium alloys and their effect on corrosion resistance in various environments, Adv. Eng. Mater. 8 (2006) 511–533, https://doi.org/10.1002/adem.200500257.
[14] G. Barati Darband, M. Aliofkhazraei, P. Hamghalam, N. Valizade, Plasma electrolytic oxidation of magnesium and its alloys: mechanism, properties and applications, J. Magnes. Alloy 5 (2017) 74–132, https://doi.org/10.1016/j.jma.2017.02.004.
[15] H.F. Guo, M.Z. An, Growth of ceramic coatings on AZ91D magnesium alloys by micro-arc oxidation in aluminate-fluoride solutions and evaluation of corrosion resistance, Appl. Surf. Sci. 246 (2005) 229–238, https://doi.org/10.1016/j.apsusc.2004.11.031.
[16] L. Wang, L. Chen, Z. Yan, H. Wang, J. Peng, Effect of potassium fluoride on structure and corrosion resistance of plasma electrolytic oxidation films formed on AZ31 magnesium alloy, J. Alloys. Compd. 480 (2009) 469–474, https://doi.org/10.1016/j.jallcom.2009.01.102.
[17] B. Kazanski, A. Kossenko, M. Zinigrad, A. Lugovskoy, Fluoride ions as modifiers of the oxide layer produced by plasma electrolytic oxidation on AZ91D magnesium alloy, Appl. Surf. Sci. 287 (2013) 461–466, https://doi.org/10.1016/j.apsusc.2013.09.180.
[18] W. Mu, Y. Han, Characterization and properties of the MgF_2/ZrO_2 composite coatings on magnesium prepared by micro-arc oxidation, Surf. Coatings Technol. 202 (2008) 4278–4284, https://doi.org/10.1016/j.surfcoat.2008.03.022.
[19] S.P. Sah, Y. Aoki, H. Habazaki, Influence of phosphate concentration on plasma electrolytic oxidation of AZ80 magnesium alloy in alkaline aluminate solution, Mater. Trans. 51 (2010) 94–102, https://doi.org/10.2320/matertrans.M2009226.
[20] A. Ghasemi, V.S. Raja, C. Blawert, W. Dietzel, K.U. Kainer, The role of anions in the formation and corrosion resistance of the plasma electrolytic oxidation coatings, Surf. Coatings Technol. 204 (2010) 1469–1478, https://doi.org/10.1016/j.surfcoat.2009.09.069.
[21] H. Ma, D. Li, C. Liu, Z. Huang, D. He, Q. Yan, P. Liu, P. Nash, D. Shen, An investigation of $(NaPO_3)_6$ effects and mechanisms during micro-arc oxidation of AZ31 magnesium alloy, Surf. Coatings Technol. 266 (2015) 151–159, https://doi.org/10.1016/j.surfcoat.2015.02.033.
[22] H. Luo, Q. Cai, B. Wei, B. Yu, D. Li, J. He, Z. Liu, Effect of $(NaPO_3)_6$ concentrations on corrosion resistance of plasma electrolytic oxidation coatings formed on AZ91D magnesium alloy, J. Alloys. Compd. 464 (2008) 537–543, https://doi.org/10.1016/j.jallcom.2007.10.072.
[23] Y. Mori, A. Koshi, J. Liao, H. Asoh, S. Ono, Characteristics and corrosion resistance of plasma electrolytic oxidation coatings on AZ31B Mg alloy formed in phosphate - Silicate mixture electrolytes, Corros. Sci. 88 (2014) 254–262, https://doi.org/10.1016/j.corsci.2014.07.038.
[24] S.V. Lamaka, G. Knörnschild, D.V. Snihirova, M.G. Taryba, M.L. Zheludkevich, M. G.S. Ferreira, Complex anticorrosion coating for ZK30 magnesium alloy, Electrochim. Acta 55 (2009) 131–141, https://doi.org/10.1016/j.electacta.2009.08.018.
[25] M. Mohedano, C. Blawert, M.L. Zheludkevich, Cerium-based sealing of PEO coated AM50 magnesium alloy, Surf. Coat. Technol. 269 (2015) 145–154, https://doi.org/10.1016/j.surfcoat.2015.01.003.
[26] D.K. Ivanoua, K.A. Yasakau, S. Kallip, A. Lisenkov, M. Starykevich, S.V. Lamaka, M. G.S. Ferreira, M.L. Zheludkevich, Active corrosion protection coating for ZE41 magnesium alloy created by combining PEO and sol-gel techniques, RSC Adv. 6 (2016) 12553–12560, https://doi.org/10.1039/C5RA22639B.
[27] A.S. Gnedenkov, S.L. Sinebryukhov, D.V. Mashtalyar, S.V. Gnedenkov, Protective properties of inhibitor-containing composite coatings on a Mg alloy, Eval. Program Plann. 102 (2016) 348–354, https://doi.org/10.1016/j.corsci.2015.10.026.
[28] Y. Chen, X. Lu, S.V. Lamaka, P. Ju, C. Blawert, T. Zhang, F. Wang, M. L. Zheludkevich, Active protection of Mg alloy by composite PEO coating loaded with corrosion inhibitors, Appl. Surf. Sci. 504 (2019), 144462, https://doi.org/10.1016/j.apsusc.2019.144462.
[29] J. Yang, C. Blawert, S.V. Lamaka, D. Snihirova, X. Lu, S. Di, M.L. Zheludkevic, Corrosion protection properties of inhibitor containing hybrid PEO-epoxy coating on magnesium, Corros. Sci. 140 (2018) 99–110, https://doi.org/10.1016/j.corsci.2018.06.014.
[30] S.V. Lamaka, B. Vaghefinazari, D. Mei, R.P. Petrauskas, D. Höche, M. L. Zheludkevich, Comprehensive screening of Mg corrosion inhibitors, Corros. Sci. 128 (2017) 224–240, https://doi.org/10.1016/j.corsci.2017.07.011.
[31] P. Visser, Y. Liu, H. Terryn, J.M.C. Mol, Lithium salts as leachable corrosion inhibitors and potential replacement for hexavalent chromium in organic coatings for the protection of aluminum alloys, J. Coatings Technol. Res. 13 (2016) 557–566, https://doi.org/10.1007/s11998-016-9784-6.
[32] A.C. Bouali, A.C. Bastos, S.V. Lamaka, M. Serdechnova, M.G.S. Ferreira, M. L. Zheludkevich, Evaporation of electrolyte during SVET measurements: the scale of the problem and the solutions, Electroanalysis. 31 (2019) 2290–2298, https://doi.org/10.1002/elan.201900435.
[33] J. Vogelsang, W. Strunz, The evaluation of experimental dielectric data of barrier coatings by means of different models, Electrochim. Acta 46 (2001) 3619–3625, https://doi.org/10.1016/S0013-4686(01)00644-2.
[34] J.B. Jorcin, M.E. Orazem, N. Pébère, B. Tribollet, CPE analysis by local electrochemical impedance spectroscopy, Electrochim. Acta 51 (2006) 1473–1479, https://doi.org/10.1016/j.electacta.2005.02.128.

[35] C.H. Kim, S. Il Pyun, J.H. Kim, An investigation of the capacitance dispersion on the fractal carbon electrode with edge and basal orientations, Electrochim. Acta 48 (2003) 3455–3463, https://doi.org/10.1016/S0013-4686(03)00464-X.
[36] R.O. Hussein, D.O. Northwood, X. Nie, The effect of processing parameters and substrate composition on the corrosion resistance of plasma electrolytic oxidation (PEO) coated magnesium alloys, Surf. Coat. Technol. 237 (2013) 357–368, https://doi.org/10.1016/j.surfcoat.2013.09.021.
[37] V. Dehnavi, B. Li, D.W. Shoesmith, X. Yang, S. Rohani, Effect of duty cycle and applied current frequency on plasma electrolytic oxidation (PEO) coating growth behavior, Surf. Coat. Technol. 226 (2013) 100–107, https://doi.org/10.1016/j.surfcoat.2013.03.041.
[38] Y. Cheng, Z. Xue, Q. Wang, X. Wu, E. Matykina, P. Skeldon, G.E. Thompson, Electrochimica Acta New findings on properties of plasma electrolytic oxidation coatings from study of an Al–Cu–Li alloy, Electrochim. Acta 107 (2013) 358–378, https://doi.org/10.1016/j.electacta.2013.06.022.
[39] X. Ma, C. Blawert, D. Höche, M.L. Zheludkevich, K.U. Kainer, Investigation of electrode distance impact on PEO coating formation assisted by simulation, Appl. Surf. Sci. 388 (2016) 304–312, https://doi.org/10.1016/j.apsusc.2016.01.030.
[40] E. Matykina, R. Arrabal, P. Skeldon, G.E. Thompson, P. Belenguer, AC PEO of aluminium with porous alumina precursor fi lms, Surf. Coat. Technol. 205 (2010) 1668–1678, https://doi.org/10.1016/j.surfcoat.2010.05.014.
[41] T.W. Clyne, S.C. Troughton, A review of recent work on discharge characteristics during plasma electrolytic oxidation of various metals oxidation of various metals, Int. Mater. Rev. 64 (2019) 127–162, https://doi.org/10.1080/09506608.2018.1466492.
[42] X. Lu, S. Prasad, N. Scharnagl, M. Störmer, M. Starykevich, M. Mohedano, C. Blawert, M.L. Zheludkevich, K. Ulrich, Degradation behavior of PEO coating on AM50 magnesium alloy produced from electrolytes with clay particle addition, Surf. Coat. Technol. 269 (2015) 155–169, https://doi.org/10.1016/j.surfcoat.2014.11.027.
[43] A. Santos-Coquillat, M. Esteban-Lucia, E. Martinez-Campos, M. Mohedano, R. Arrabal, PEO coatings design for Mg-Ca alloy for cardiovascular stent and bone regeneration applications, Mater. Sci. Eng. C. 105 (2019), 110026, https://doi.org/10.1016/j.msec.2019.110026.
[44] M. Mohedano, B.J.C. Luthringer, B. Mingo, F. Feyerabend, R. Arrabal, P.J. Sanchez-egido, C. Blawert, Bioactive plasma electrolytic oxidation coatings on Mg-Ca alloy to control degradation behaviour, Surf. Coat. Technol. 315 (2017) 454–467, https://doi.org/10.1016/j.surfcoat.2017.02.050.
[45] J. Dou, Y. Zhao, L. Lu, G. Gu, H. Yu, C. Chen, Effect of the second-step voltages on the structural and corrosion properties of silicon – calcium – phosphate (Si–CaP) coatings on Mg–Zn–Ca alloy, R. Soc. Open Sci. 5 (2018), 172410, https://doi.org/10.1098/rsos.172410.
[46] R. Arrabal, E. Matykina, A. Pardo, M.C. Merino, K. Paucar, M. Mohedano, P. Casajús, Corrosion behaviour of AZ91D and AM50 magnesium alloys with Nd and Gd additions in humid environments, Corros. Sci. 55 (2012) 351–362, https://doi.org/10.1016/j.corsci.2011.10.038.
[47] S. Agathopoulos, D.U. Tulyaganov, J.M.G. Ventura, S. Kannan, A. Saranti, M. A. Karakassides, J.M.F. Ferreira, Structural analysis and devitrification of glasses based on the CaO–MgO–SiO_2 system with B_2O_3, Na_2O, CaF_2 and P_2O_5 additives, J. Non. Solids 352 (2006) 322–328, https://doi.org/10.1016/j.jnoncrysol.2005.12.003.
[48] S. Peng, M. Li, J. Wang, Q. Tian, S. Wang, B. Tang, Corrosion behavior and biological activity of micro-arc oxidation coating with puerarin on pure magnesium surface, Results Phys 12 (2019) 1481–1489, https://doi.org/10.1016/j.rinp.2019.01.021.